Stanford Exploration Project, Report 75, November 17, 1997, pages 271–293

Modeling reflections from the Austin Chalk – a practical application of azimuthal anisotropy

[1]

Martin Karrenbach, Dave Nichols & Francis Muir[2]

keywords: *amplitudes, modeling, anisotropy, velocity, slant stack, density*

ABSTRACT

If a rock has elastic properties that vary with azimuth, then reflections from such a rock will likewise. We examine a simple situation where a homogeneous model material – representing a shale – overlies another homogeneous model material which simulates an isotropic chalk matrix and a set of vertical fractures with constant azimuth. Our modeling illustrates the small variability in azimuthal reflectivity as the amount of fracturing is increased, and also how reflection strength is affected by the nature of the fluid inclusion – gas or liquid.

INTRODUCTION

Amplitude Verus Offset analysis (AVO) assuming isotropic media is a tool which has been known for many years (Ostrander, 1984). However little has been published so far about anisotropic treatment of AVO behaviour. While in some cases anisotropic AVO behaviour can be explained by an equivalent isotropic medium for a given azimuth; the azimuthal variation is a better indicator reflectivity changes. In some cases amplitude variations cannot be explained by an equivalent isotropic medium. We focus on a particular simple anisotropic case which is relevant in real data, since it can be produced by very finely layering isotropic material or by fracturing an isotropic rock. We use Austin Chalk as our practical example and derive material stiffnesses from data published by White (1982) and Wright (1987). We model reflections from Austin Chalk, where a transverse isotropic shale overlies chalk, with varied amounts of fracturing. We investigate wether we can practically determine fracture parameters and/or fracture content from azimuthal variations of reflectivity and find that we get measurable small indications when using converted wave modes or when going to very large offsets.

[1]given as a poster paper at the SEG/EAEG workshop on AVO 1992

[2]**email:** not available

Using a macro model description of the fractured and finely layered medium, we can employ a modeling method which works efficiently on a large – the actual surface seismic – measurement scale. Thus we avoid calculating all the fine details which are averaged out during the wave propagation process and use a homogeneous average medium that includes the macroscopic effects of microscopic fluctuations.

We address issues of: (a) how do we include the effect of fractures on the material properties, and (b) how do we carry out the modeling procedure. We choose a model with a single interface: a block of transverse isotropic (TI) shale lies over a fractured chalk. The source is located 1 km above the interface and a surface seismic survey is modeled with a large aperture (¡60 deg.). The chalk fracturing is calculated using Hudson's theory combined with Schoenberg & Muir group theory (S&M) (Nichols, 1989; Schoenberg and Muir, 1989). The regime of validity of those theories limits us to low crack density and small crack aspect ratios.

Anisotropic Finite Differences (FD) are used to model wave propagation through an anisotropic medium. We chose to test whether FD modeling of reflection amplitudes is adequate by comparing it to an analytical solution. We use this example to calibrate our method before applying it to real data in arbitrary complex media. The reflection amplitudes produced by the FD modeling are in nearly perfect agreement with analytical solutions for the reflection amplitudes (i.e. Zoeppritz, for a single flat reflector).

Using S&M equivalent medium theory, we "add" fractures to the chalk rock matrix. The vertical cracks have a constant azimuth along the inline direction. We compare inline and crossline reflection amplitude effects produced by the fracturing. Amplitude analysis is carried out in the slant-stack domain. We use a least-squares "optimum" stack to get an aperture-compensated estimate of the modeled data. Travel time curves in the slant-stack domain of the TI medium can be calculated directly or after anisotropic velocity analysis. Reflected amplitudes are extracted within a centered window along that curve. Alternatively, a downward continuation in the slant- stack domain can replace the previous process.

"ADDING" FRACTURES:

S&M limited slip interace model

In the Schoenberg & Muir formalism, fractures are treated as very thin compliant layers. The fracture filling material is assumed to be softer than the background material. The elastic moduli of the fracture are much smaller than a typical non-zero modulus of the background material. In deriving the effect of fractures, it is assumed that the fracture moduli are of the order of volume fraction of the fractures. As the thickness of the fracture layers become small, they act as linear slip interfaces. The S&M formalism can be used to "add" cracks to a given rock.

Hudson's model

Hudson's model (Nichols, 1989) of the elastic properties of fractured rocks is based on an equation for the mean field in a solid with a random distribution of inclusions. We consider Hudson's model only to first order in crack density of penny-shaped cracks. This is equivalent to only allowing single scattering and ignoring crack/crack interactions. For this approximation to hold, the crack density must be low. Hudson's formalism can be directly presented in S&M group formalism.

Limitations

Both formulations (Hudson and S&M) are valid in a regime of small volume density of cracks and a small crack aspect ratio. Our modeling examples fall within those limits. However, the Austin Chalk may in reality still have a higher volume density of cracks than what we show in our examples. Our results should be taken as a lower crack-density bound estimate.

MODEL

Figure 1 depicts the two-layer model and the 3-D-recording geometry. An equivalent homogeneous block of finely layered shale is situated on top of a homogeneous fractured chalk layer. We employ a P-source and three-component receivers about 1 km above the interface. A surface seismic survey is modeled with a large aperture. The chalk fracturing is calculated using Hudson's theory combined with Schoenberg & Muir group theory. The actual stiffness coefficients can be found in Appendix A. The unfractured elastic constants were derived from constants published by Wright (1987). Using a macro model description of the fractured chalk and finely layered shale, we can employ a FD modeling method which works efficiently on a large – the actual surface seismic – measurement scale.

FINITE DIFFERENCE METHOD

Finite differences are used to model wave propagation through an anisotropic medium. The method is described in more detail in this report (Dellinger et al., 1992). In a recent report Cunha (1991) described a modeling scheme which takes discontinuities in medium properties into account by applying different FD operators to the wavefield and the medium. Different implementations of a staggered grid or derivatives can influence the accuracy of reflection responses. In this paper, we are not employing his method, but rather use cascaded derivative operators. As can be seen from Figure 2, the reflection amplitudes produced by our modeling scheme are in nearly perfect agreement with analytical solutions to the reflection amplitudes. Figures 3 and 4 show the analytically calculated responses compared with the modeled extracted responses.

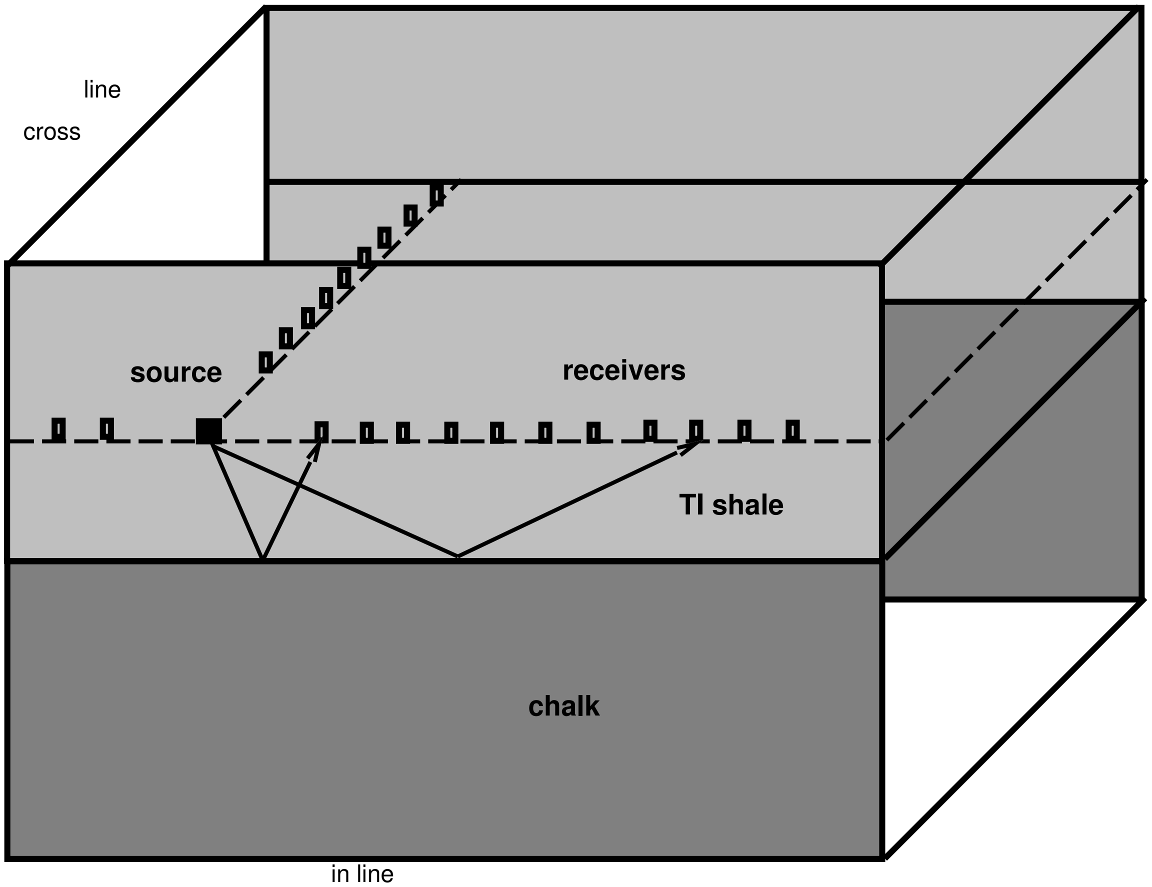

Figure 1: A homogeneous block model with inline and crossline recording. martin1-model [NR]

Such a test is clearly necessary, if we want to make sure the modeling algorithm

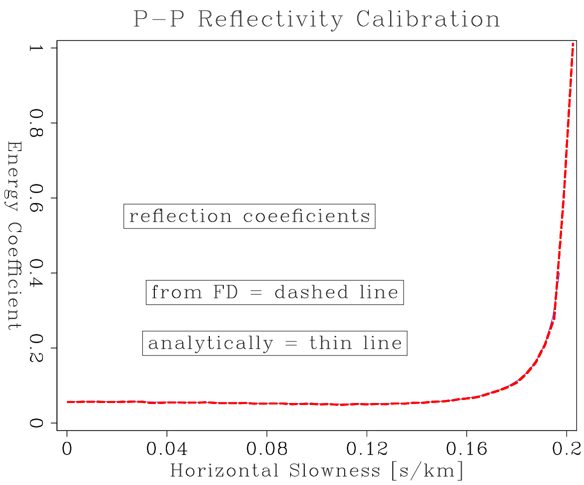

Figure 2: PP calibration curve for the FD modeling response. Reflection amplitudes were extracted using the dual experiment. Zoeppritz plane-wave energy reflection coefficients are calculated analytically. martin1-ppcalibrate [NR]

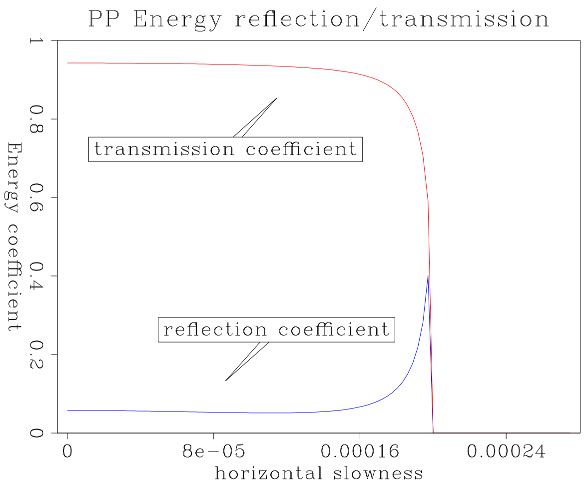

Figure 3: Analytically calculated energy reflection and transmission coefficients from Zoeppritz equations. martin1-iso1.ref [NR]

produces correct reflection coefficients at medium interfaces. The above test gives us confidence in the modeling algorithm for this type of blocky model.

Using S&M equivalent medium theory, we "add" fractures to the chalk-rock matrix. The cracks are vertical and have a constant azimuth along the inline direction. We generally compare inline and crossline amplitude effects produced by the fracturing. Amplitude analysis is carried out in the slant-stack domain.

AMPLITUDE EXTRACTION

Reflection amplitudes at the interface are retrieved by operating in the $\tau - p$ domain. Looking at the recorded time domain CMP records (Figures 5 and 6) we see an amplitude estimation problem near 1.75 sec caused by triplicating branches of reflection hyperbolae. Transforming those records to the $\tau - p$ domain gets rid of triplications and provides a robust estimate of the "phase domain" representation of the reflected

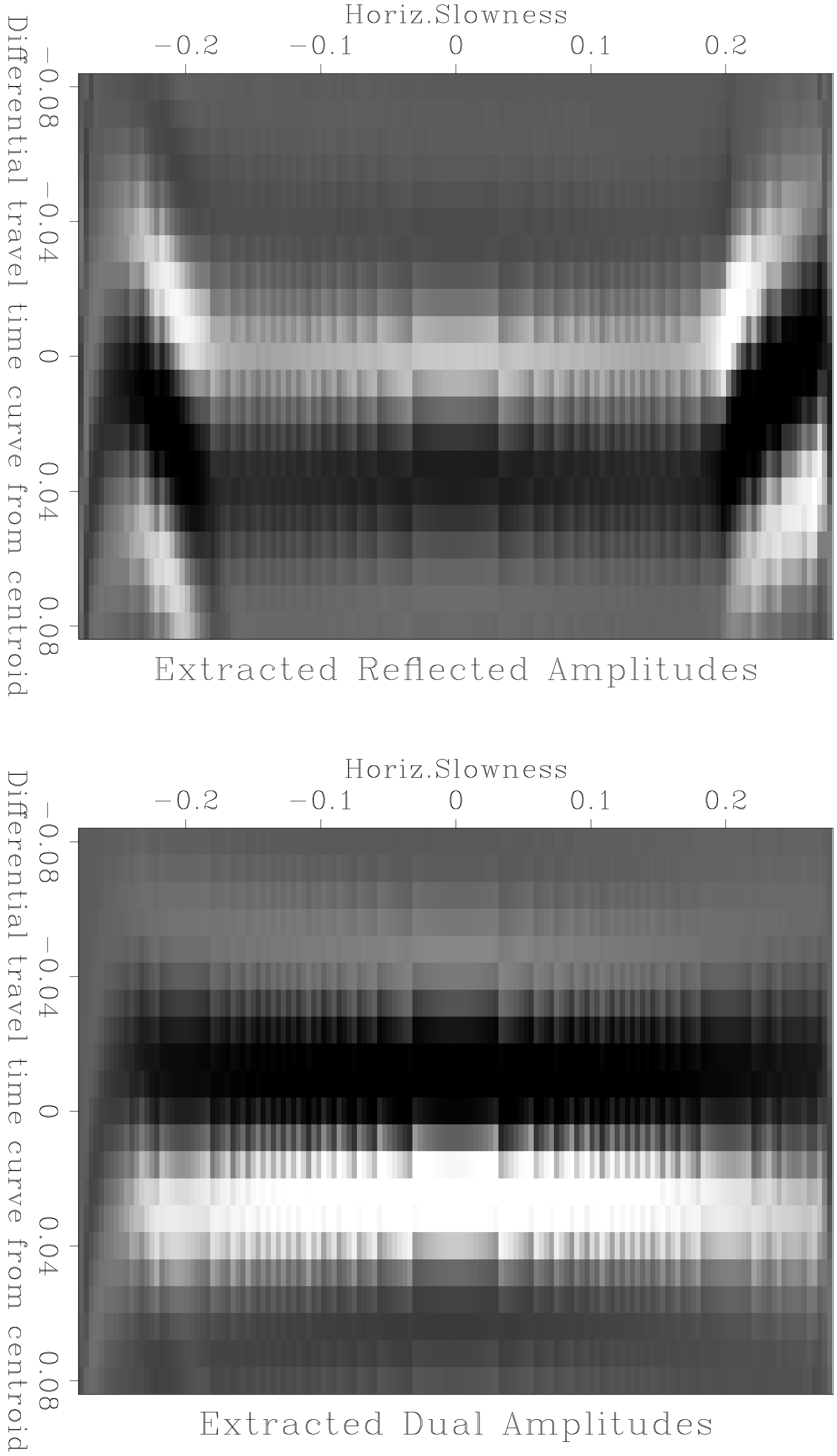

Figure 4: Extracted amplitudes from the FD modeling experiment and the dual experiment. The dual experiment estimates all propagation effects but omits reflection at the boundary. For that reason the two signals have different phases. martin1-extraiso [NR]

waves in an anisotropic medium. Thus the traveltime curves in the $\tau - p$ domain are simple curves. From a practical point of view the slant-stack domain offers more advantages such as, dealiasing (Nichols, 1992), aperture and geometry compensated estimates of the wave field (Kostov, 1990), and regridding (inteerpolation) capabilities. The events of interest in Figures 7 and 8 (inline) are the uppermost two elliptical curves corresponding to the PP and PS reflection from the shale/chalk interface. The slant-stack difference sections, obtained by subtracting the crossline slant-stack section from the inline counterpart gives Figure 9 and 10. The differences are obvious at values close to critical horizontal slowness, and at the triplicating event for a large array of horizontal slowness values.

The first step in amplitude extraction is to transform the CMP gathers into the τ-p space using an "optimum" least-squares procedure, aiming to give us an unbiased, amplitude preserving estimate of the wave field. The traveltimes in the slant-stack domain are skewed ellipses in the anisotropic case. Since we are interested in PP and PS reflection, it is useful to write the Double Square Root (DSR) equation in the τ-p domain. The DSR equation

$$\tau = \frac{z_0}{v_{down}} \sqrt{(1 - p^2 v_{down}^2(p))} + \frac{z_0}{v_{up}} \sqrt{(1 - p^2 v_{up}^2(p))} \tag{1}$$

is a sum of two skewed square roots. Here the velocity depends on the ray parameter, but may not vary laterally. If v_{down} is not identical to v_{up}, we are calculating the traveltime for a mode-converted wave. Amplitudes can then be extracted along a prescribed corridor given by the τ-p traveltime curve in conjunction with the dominant wavelet period. From those extracted values the amplitude at the centroid frequency is picked. This gives us a robust reflection energy estimate for a given definite wave type.

RESULTS

Using S&M group theory to add fractures to the chalk matrix, we obtain the phase velocity curves in Figure 13 as polar plots. The fractures are vertical and have constant azimuth along the inline direction. So we have a preferred inline-fracture orientation with a horizontal axis of symmetry. Examine just the resulting P-wave velocity. The solid line is the unfractured chalk velocity and it shows an isotropic response. Looking at the neighboring dashed lines, the fractured P velocities (4-5 km/s), the inline and crossline velocities coincide for purely horizontal propagation and up to 45 degrees from the horizontal. The discrepancy increases from there on and for purely vertical propagation until the inline and crossline differences reach a magnitude of 0.8 km/s. The shear waves exhibit similar behaviour, but the magnitude of those effects are generally smaller. Reflection amplitude behaviour at the interface will depend on both the stiffnesses above and below. So even if we see a strong anisotropy in velocity in one medium, there is still no guarantee that we will get a strong reflection amplitude anisotropy, since the other medium could vary in the same manner and the differences could be small.

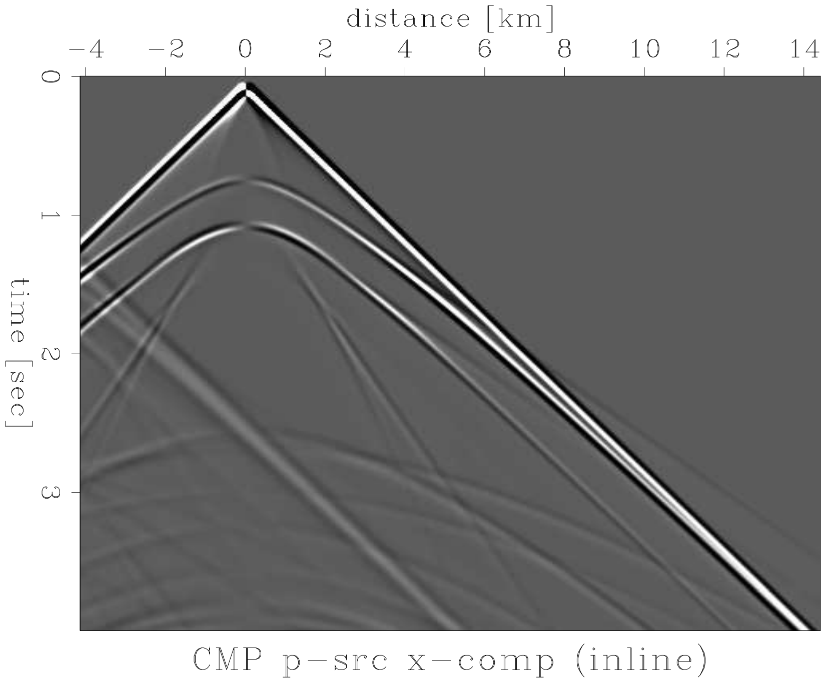

Figure 5: Recorded seismograms from a p-source into an x-component. martin1-pxseis.f10.0.cmp.SUB [NR]

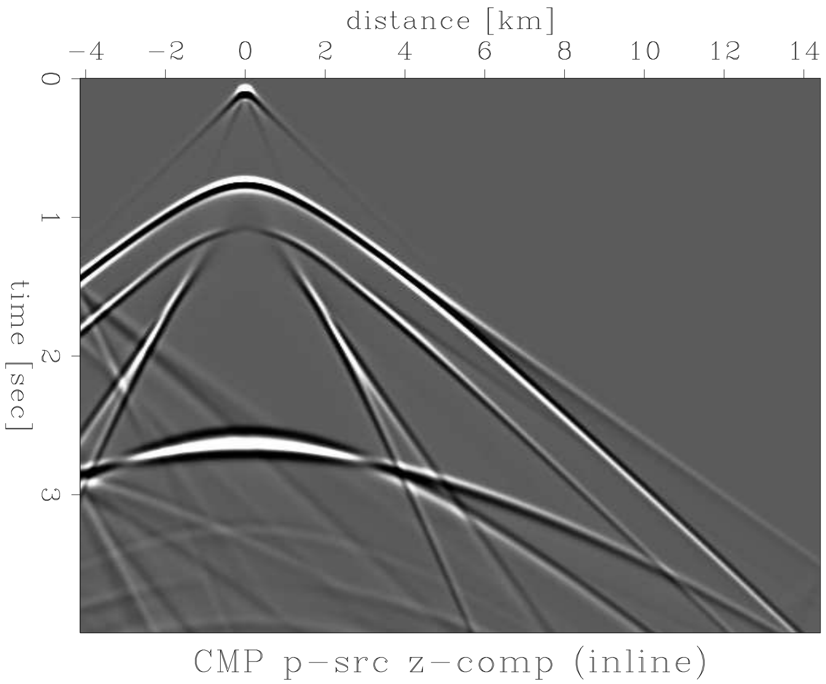

Figure 6: Recorded seismogram from a p-source into an x-component. martin1-pzseis.f10.0.cmp.SUB [NR]

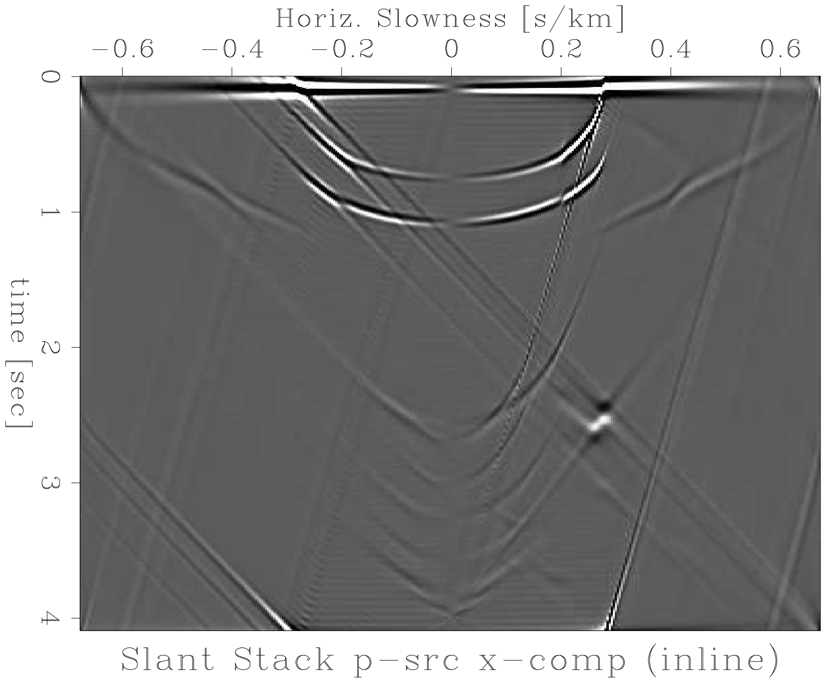

Figure 7: The CMP gather (Fig. 5) is transformed using a least-squares slant-stack. martin1-pxseis.f10.0.cmp.SUB.SL [NR]

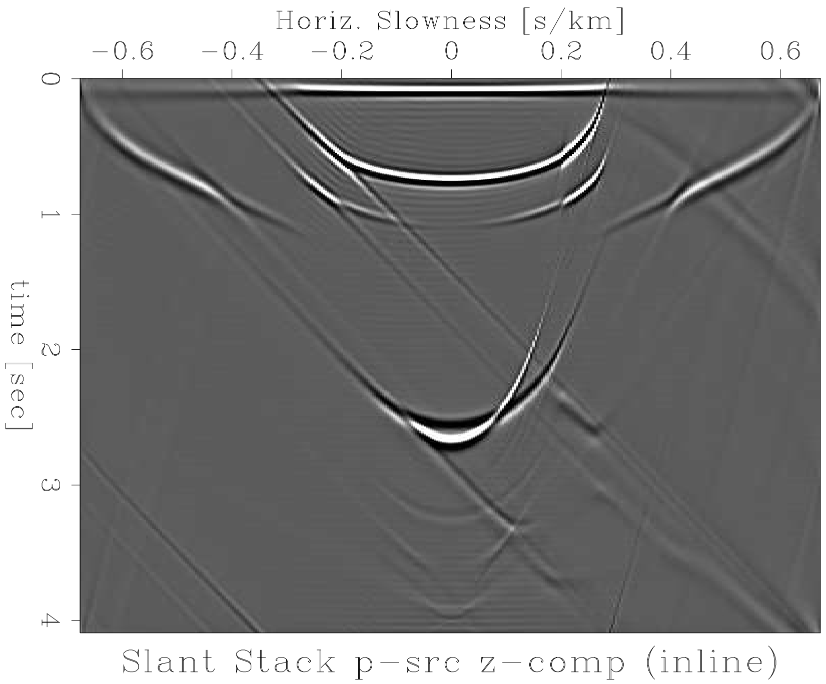

Figure 8: The CMP gather (Fig. 6) is transformed using a least-squares slant-stack. martin1-pzseis.f10.0.cmp.SUB.SL [NR]

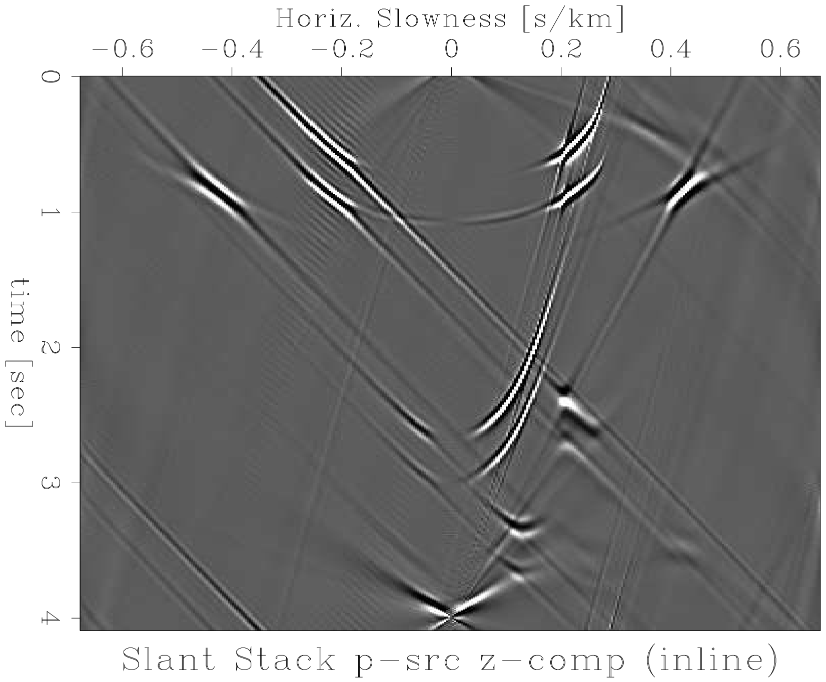

Figure 9: Subtraction of inline and crossline slant-stacks. $\boxed{\text{martin1-pxseis.f10.SL.DIFF}}$ [NR]

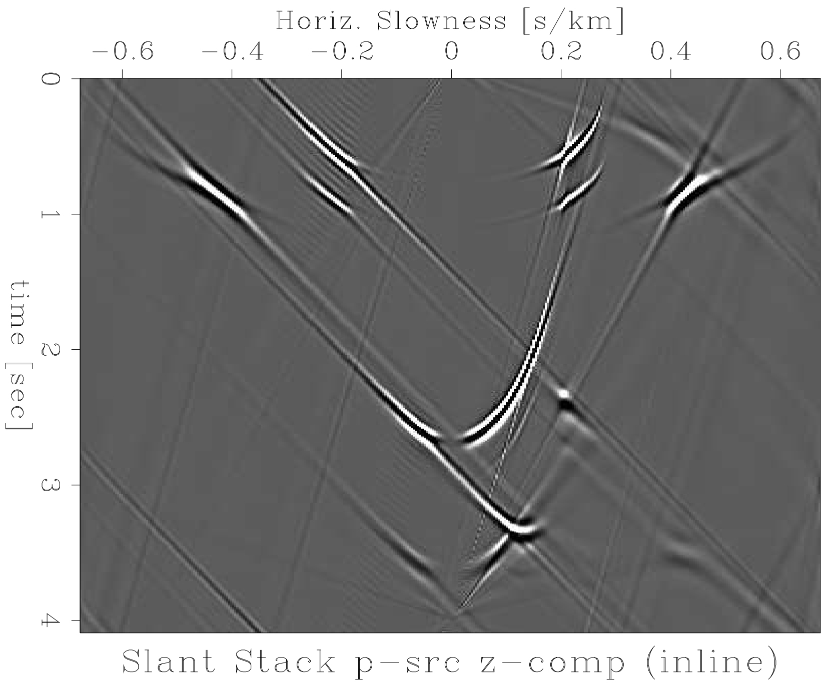

Figure 10: Subtraction of inline and crossline slant-stacks. $\boxed{\text{martin1-pzseis.f10.SL.DIFF}}$ [NR]

Figures 11 and 12 show inline and crossline reflection amplitude comparisons. Very small differences exist for the PP reflection angles less than the critical angle. Approaching the critical angle, the reflection amplitudes show distinct changes between inline and crossline behaviour. The same is true for the PS reflection with the differences showing up at even smaller propagation angles. The most important effect, however, is the azimuthal change in critical angle. If we had designed an experiment to record out to the PS critical angle, that would give us the clearer information about anisotropy. However, for targets of interest one usually has precritical amplitudes available. Figures 11 and 12 tell us that the mode converted PS wave has a better chance in estimating the magnitude of anisotropy. Figure 14 shows again phase velocity curves as a scalar plot. These plots differ from Figure 13 in that the cracks are now fluid filled, while before they were unfilled voids; they show a decrease in the difference of the velocity curves.

Figures 15 and 16 are computed by incorporating not just a bulk excess compliance, but Hudson's approximation expressed in the S&M group domain (Nichols, 1989). These two pictures show for the PP azimuthal amplitude only small differences close to the critical angle, but the PS difference is now more pronounced, also influencing the position of the critical angle slightly.

Hudson's theory allows the variation of three parameters: the aspect ratio, the stiffness of the filling material, and the volume density of cracks. In the following examples, the crack filling material stiffness (a fluid) is maintained constant. First we consider a large aspect ratio and medium volume density. This model is an extreme example, and pushes the validity of our crack model. The P-wave sees a different bulk modulus, especially when compared to Figure 23. Figure 17 shows the corresponding polar plots of phase velocity curves. The solid lines denote inline velocity curves. Comparing the P-wave velocities inline and crossline, we see no difference for horizontal propagation but some differences at other angles. The difference reverses sign along the propagation curve and is largest for near vertical propagation. The S-wave propagation exhibits somewhat different behaviour, but the effects are of similar magnitude. PP amplitude differences mainly show up near the PS critical angle. In the PS mode converted wave, we see the inline-crossline amplitude difference changing sign going from near vertical to PS critical angle propagation. We would expect this since the phase velocity curves crossing over in Figure 17. Again the PS critical angle is shifted with respect to the inline angle.

Next we consider in Figure 20 a chalk and go to the other extreme, compared to Figure 17 and crack it with a small aspect ratio, but giving a large volume density of fluid-filled cracks. We have many long, thin fluid-filled cracks (Fig. 20). The large crack volume density lets us expect that the P-wave can traverse the chalk matrix relatively unobstructed in any direction (less azimuthal dependence). The shear wave however sees more displacement discontinuities due to the fluid inclusion over a much greater range of angles. For Figure 20, the P-waves show only minor azimuthal differences at medium propagation angles. The PP reflection amplitude in Figure 21 shows hardly any differences inline and crossline. The PS converted mode (Figure

22), however, shows more variability, with the differences now exhibiting a constant sign for all angles. Most importantly we recognize that the critical angle stays the same for inline and crossline experiments. In that case the PS critical angle does not give us any information about anisotropy.

The final example is a chalk matrix with a medium aspect ratio and a small volume density of cracks (Figure 23). This is well within the validity limits of the theory. For fluid inclusion the reflection amplitudes in Figure 26 and 27 show hardly any sign of azimuthal amplitude variation. With a gas filling, the difference between inline and crossline appears again for PP as well as for converted mode PS reflections. The PS critical angle is shifted from inline to crossline. In this sense, discrimination between gas and fluid-filled cracks may be possible, but the ability to distinguish anisotropic from an isotropic behaviour is not guaranteed by looking only at inline and crossline experiments.

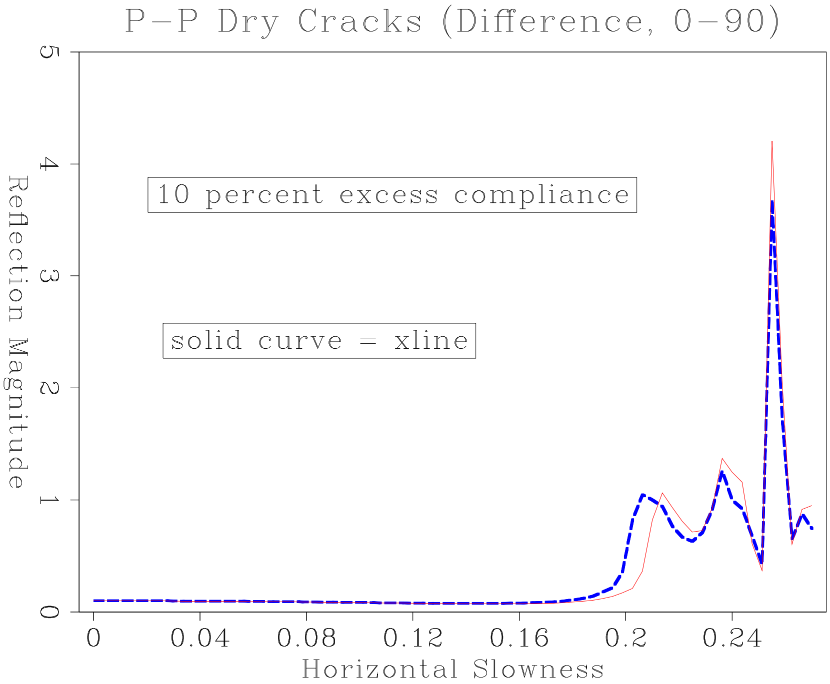

Figure 11: PP reflection amplitude comparing inline and crossline. martin1-comp.f10.pp.tp [NR]

As shown by the above examples, we can give some estimation of the crack content and distribution by looking at azimuthal variation of reflection amplitudes. This analysis is different from just looking at constant azimuth reflection amplitudes, as is done in “conventional” 2-D AVO studies. In such constant azimuth studies, the search for anisotropy does not make much sense. We can always model the anisotropic AVO beautifully, but the problem lies in the inverse process, namely to estimate anisotropy from constant azimuth AVO. In that case an isotropic equivalent medium can give the same answer for a surface seismic experiment as an anisotropic medium. In this paper we have looked only at azimuthal variations and not at the “absolute” AVO

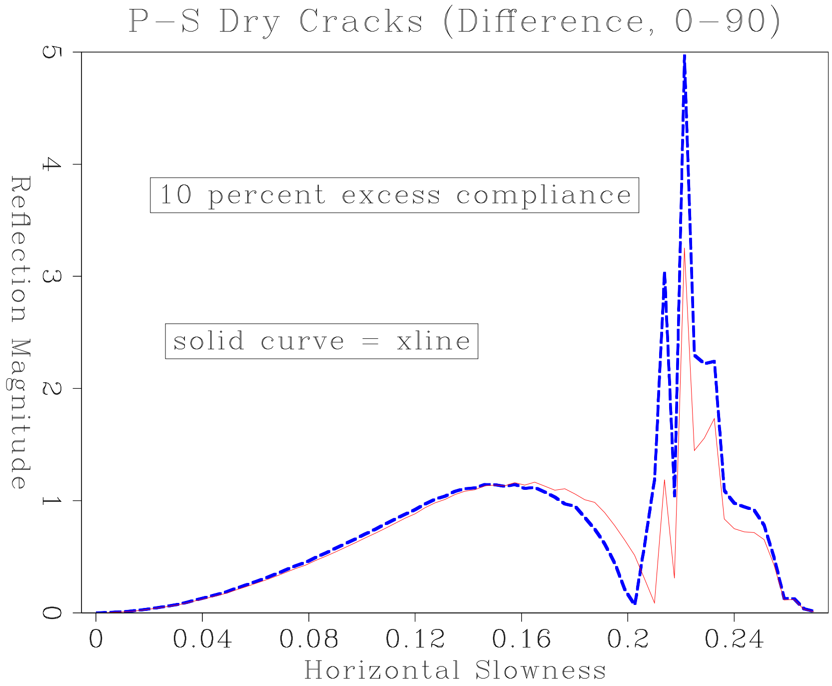

Figure 12: PS reflection amplitude comparing inline and crossline. martin1-comp.f10.ps.tp [NR]

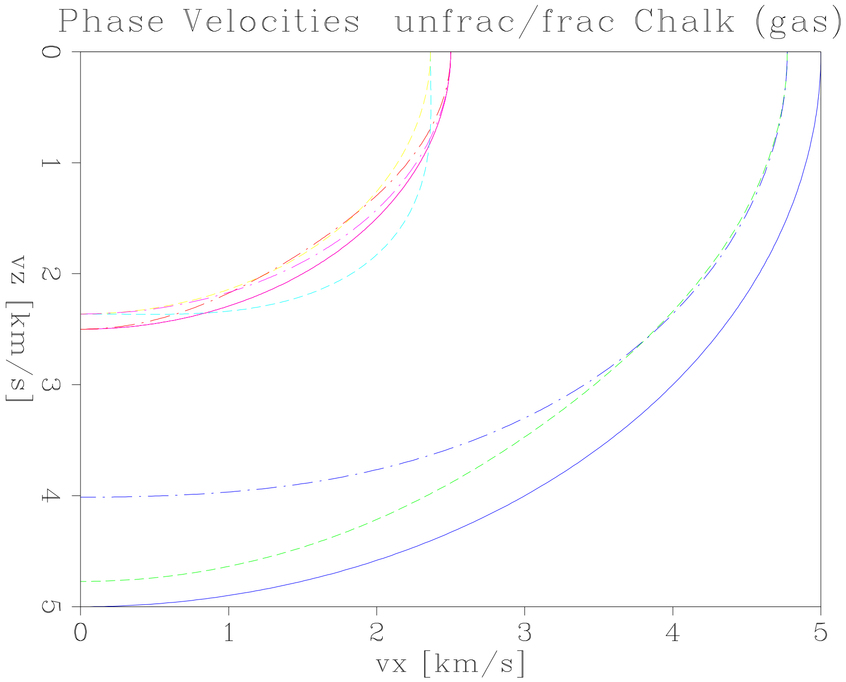

Figure 13: Velocity comparison for inline, and crossline for all three wave types. martin1-vel.unfrac.gas [NR]

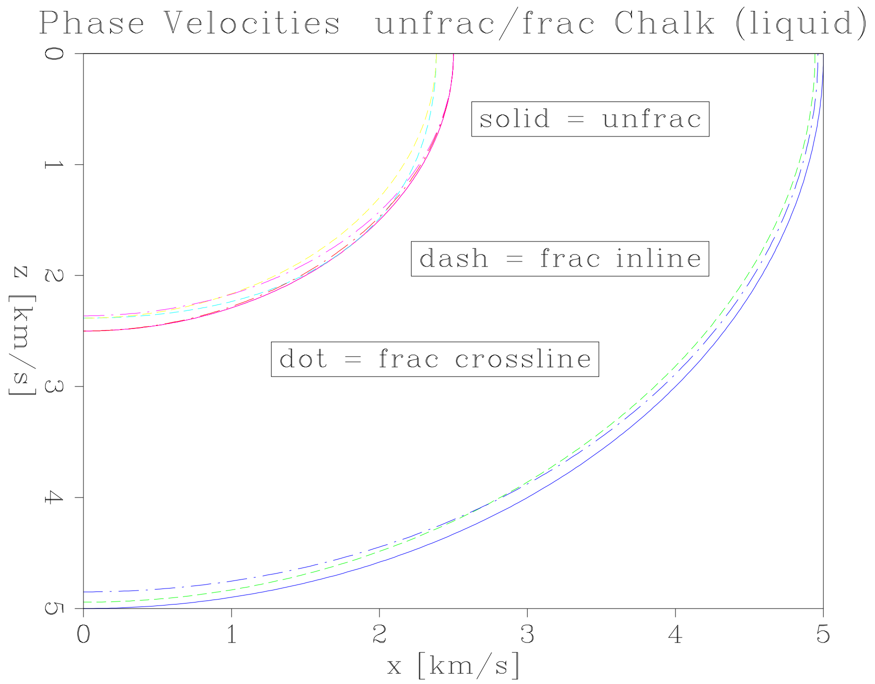

Figure 14: Velocity comparison for inline, and crossline for all three wave types. martin1-vel.unfrac.wet [NR]

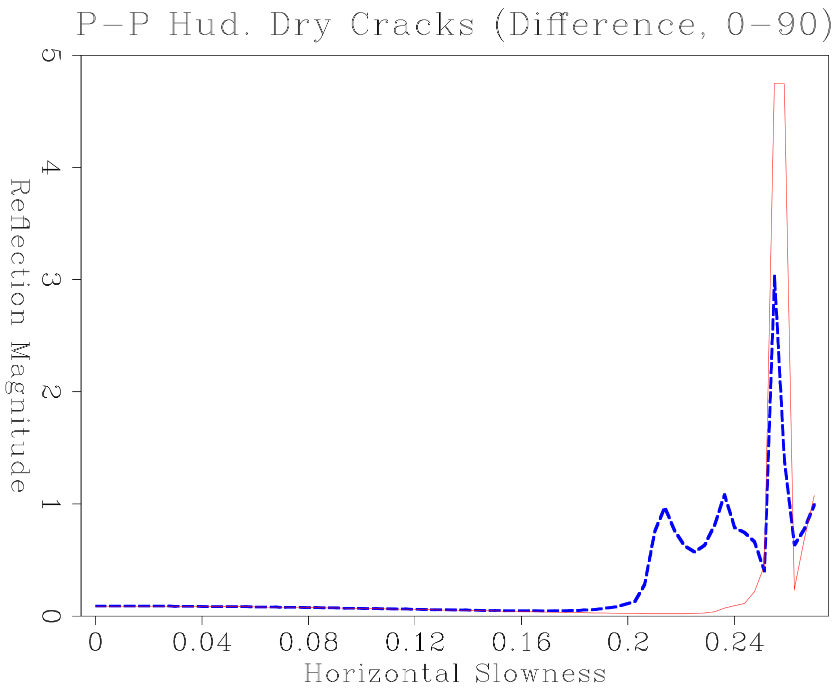

Figure 15: PP reflection amplitude comparison inline and crossline for dry cracks. Excess compliance was added using S&M formalism to generate vertical cracks. martin1-comp.f10.huddry.pp.tp [NR]

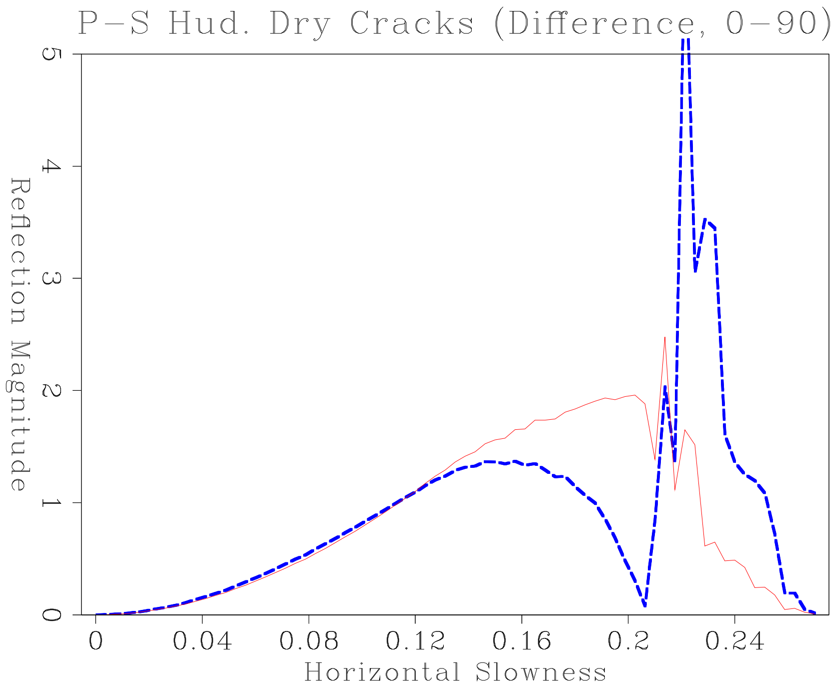

Figure 16: PS reflection amplitude comparison inline and crossline for dry cracks. Excess compliance was added using S&M formalism to generate vertical cracks. martin1-comp.f10.huddry.ps.tp [NR]

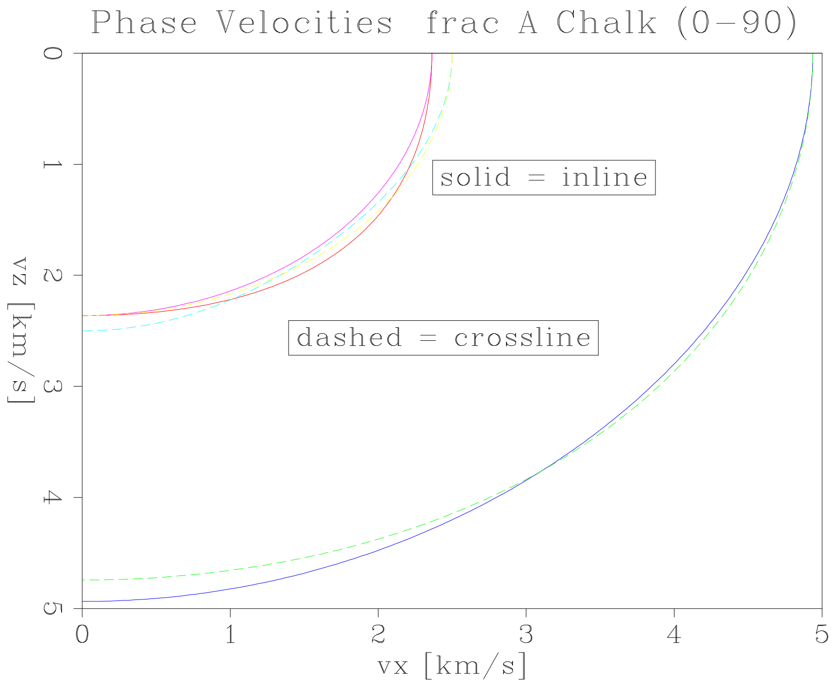

Figure 17: Phase velocity comparison for all wave types, inline and crossline. Fracture parameters are large aspect ratio and medium volume density. martin1-vel.A [NR]

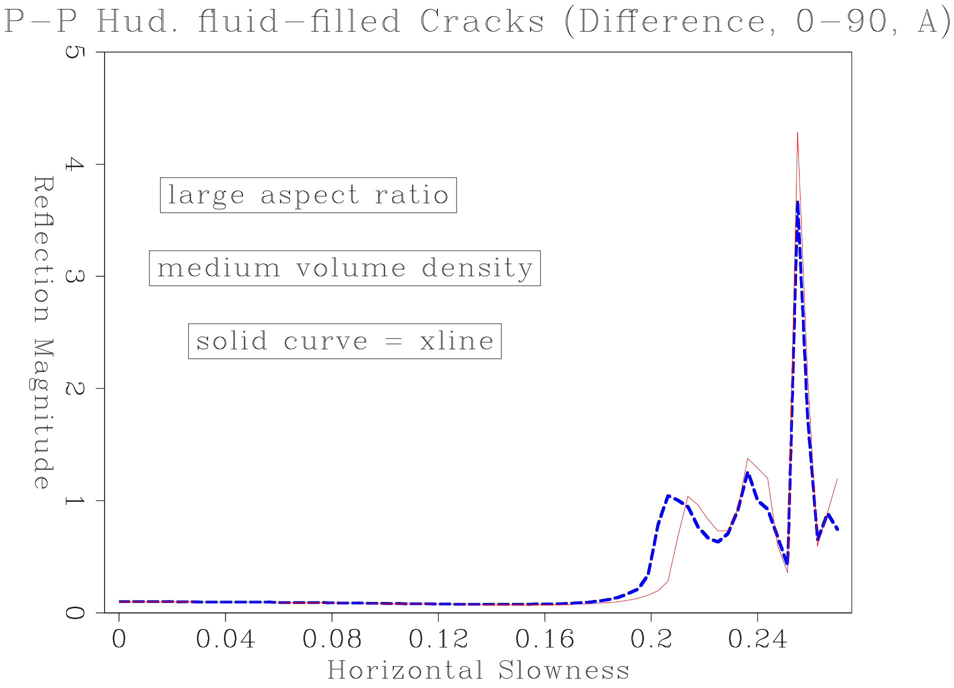

Figure 18: PP reflection amplitude comparison of inline and crossline for fluid-filled cracks. martin1-comp.A.hudwet.pp.tp [NR]

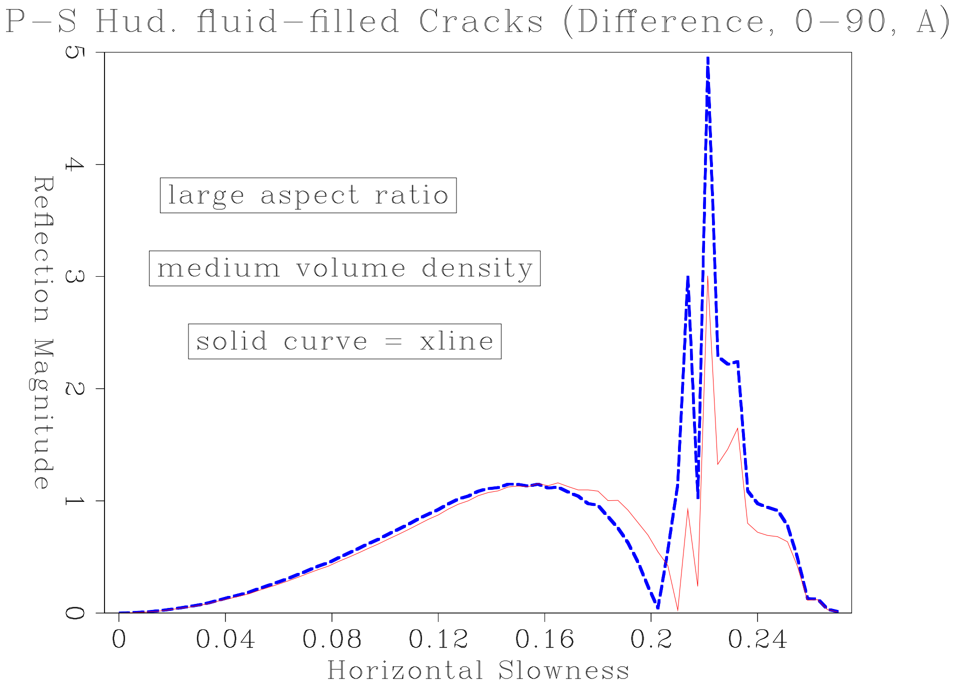

Figure 19: PS reflection amplitude comparison of inline and crossline for fluid-filled cracks. martin1-comp.A.hudwet.ps.tp [NR]

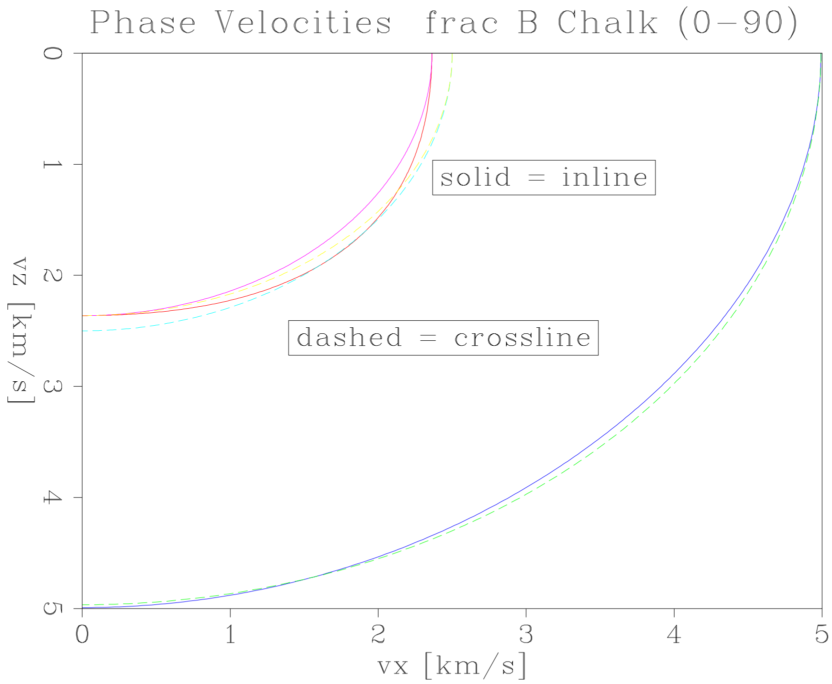

Figure 20: Phase velocity comparison for all wave types, inline and crossline. Fracture parameters are small aspect ratio and large volume density. martin1-vel.B [NR]

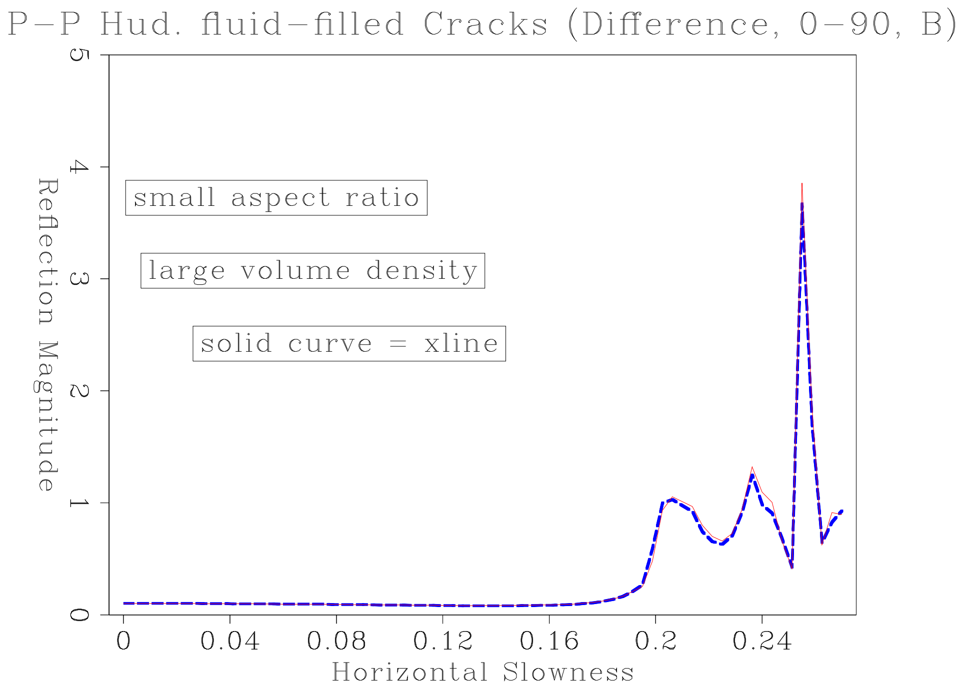

Figure 21: PP reflection amplitude comparison of inline and crossline for fluid-filled cracks type B. martin1-comp.B.hudwet.pp.tp [NR]

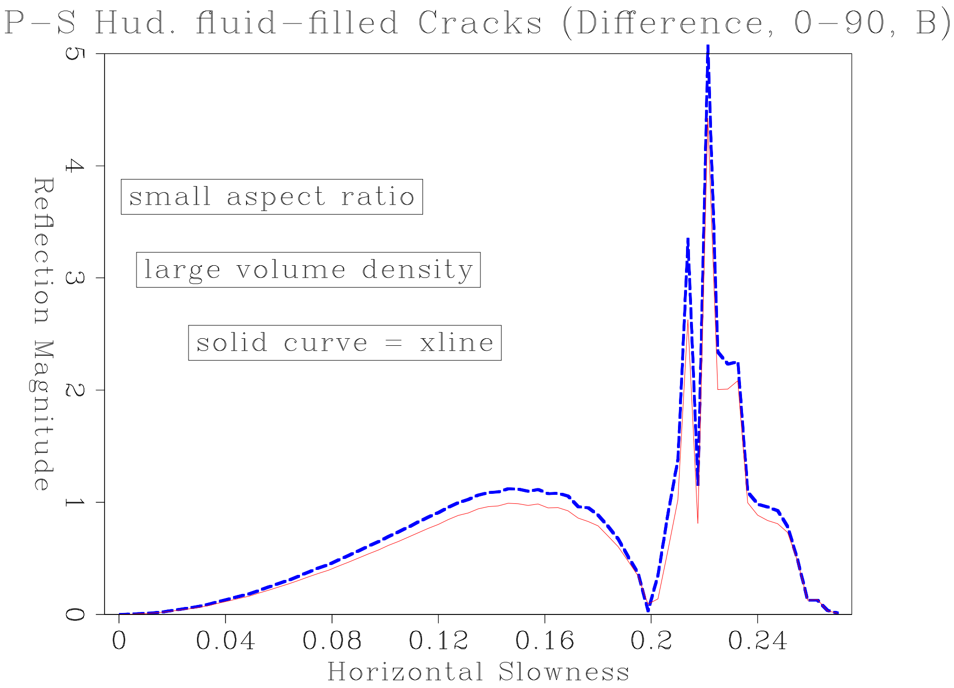

Figure 22: PS reflection amplitude comparison of inline and crossline for fluid-filled cracks type B. martin1-comp.B.hudwet.ps.tp [NR]

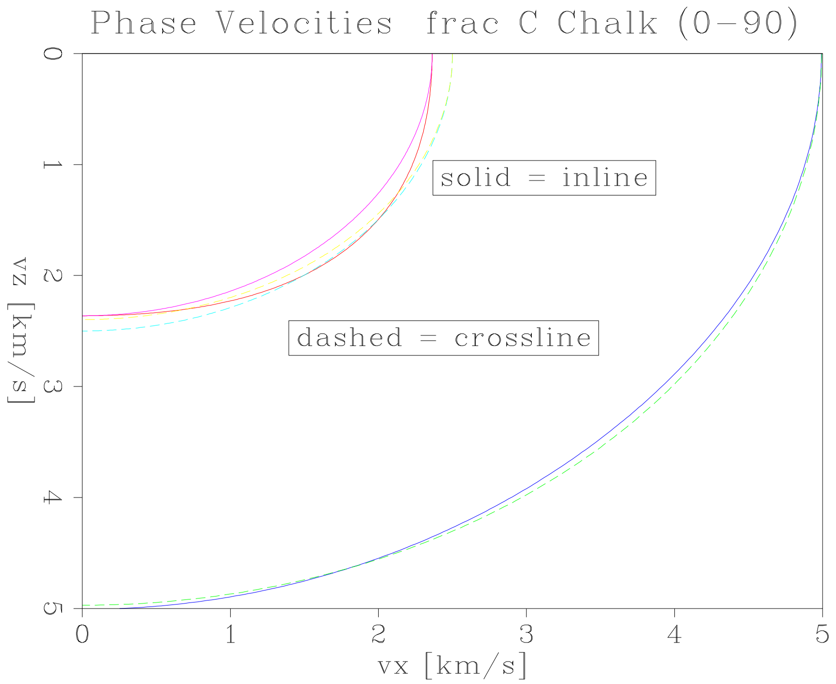

Figure 23: Phase velocity comparison for all wave types, inline and crossline. Fracture parameters are medium aspect ratio and small volume density. martin1-vel.C [NR]

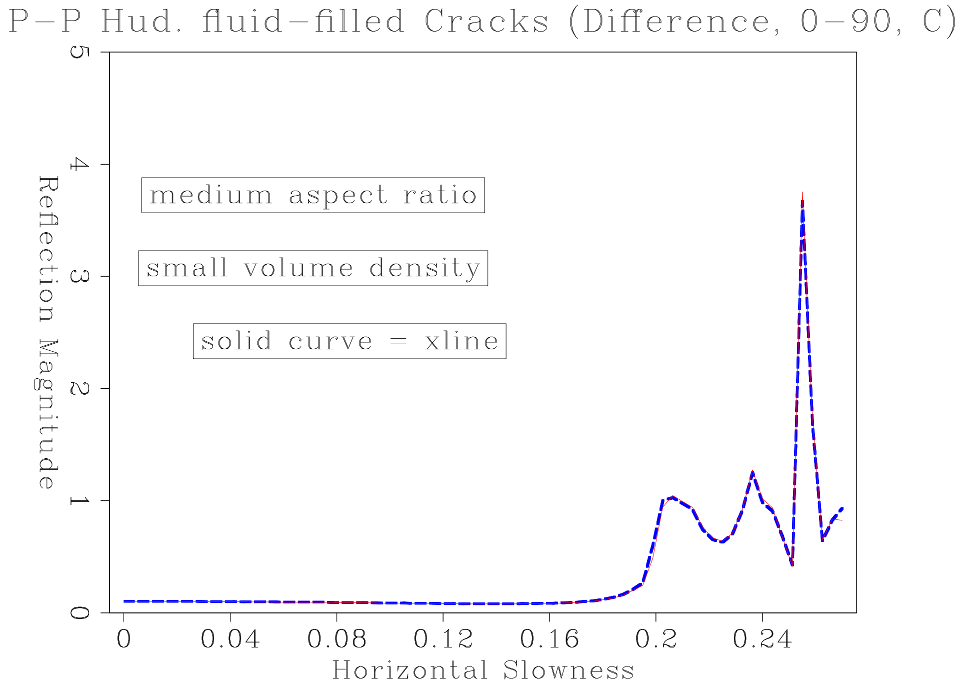

Figure 24: PP reflection amplitude comparison of inline and crossline for fluid-filled cracks of type C. martin1-comp.C.hudwet.pp.tp [NR]

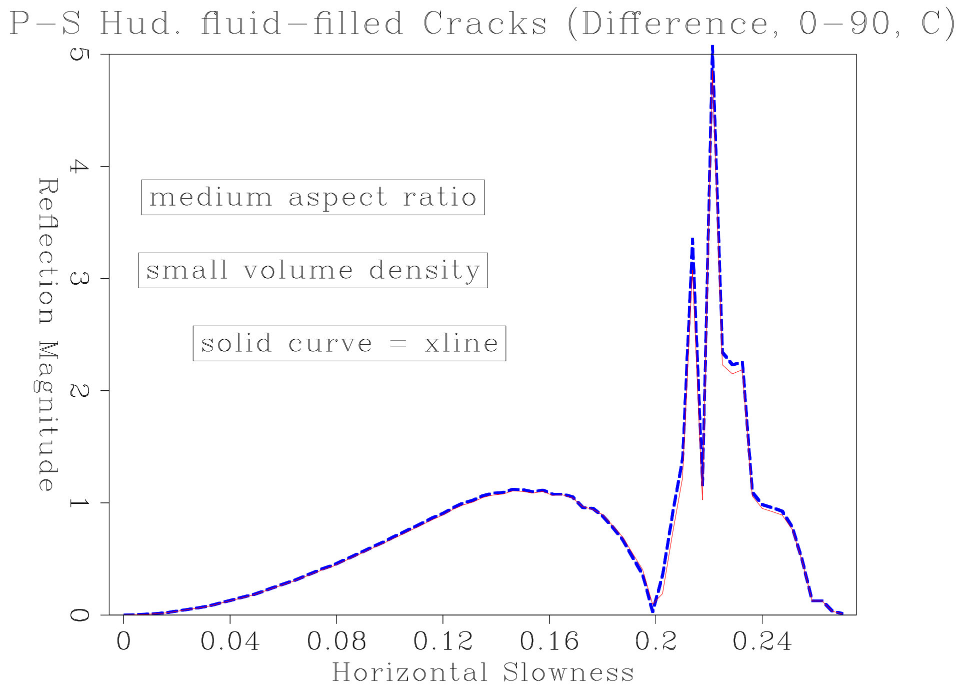

Figure 25: PS reflection amplitude comparison of inline and crossline for fluid-filled cracks of type C. martin1-comp.C.hudwet.ps.tp [NR]

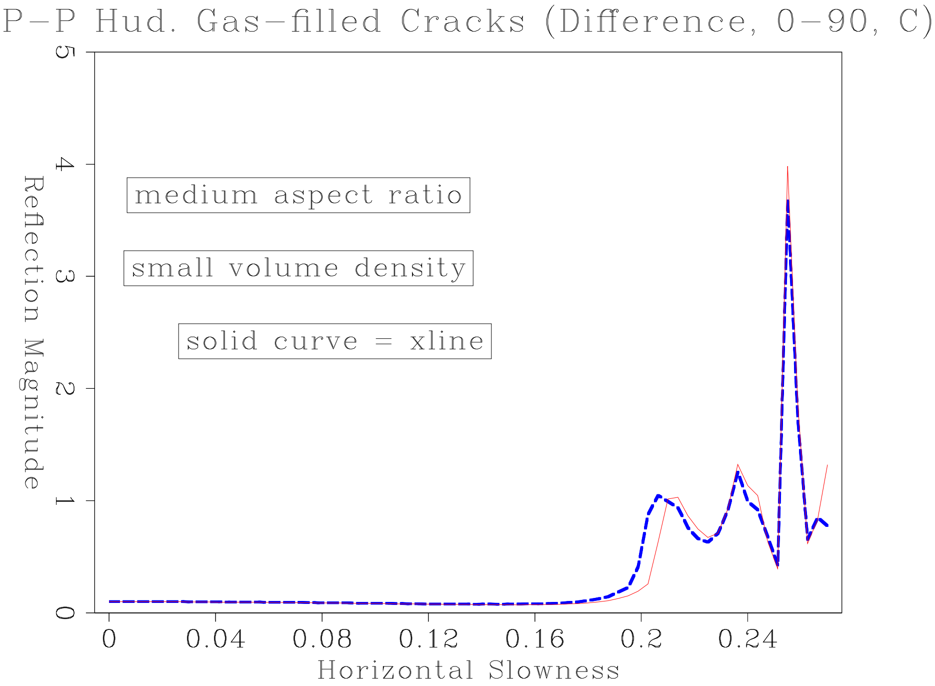

Figure 26: PP reflection amplitude comparison of inline and crossline for dry cracks type of C. martin1-comp.C.huddry.pp.tp [NR]

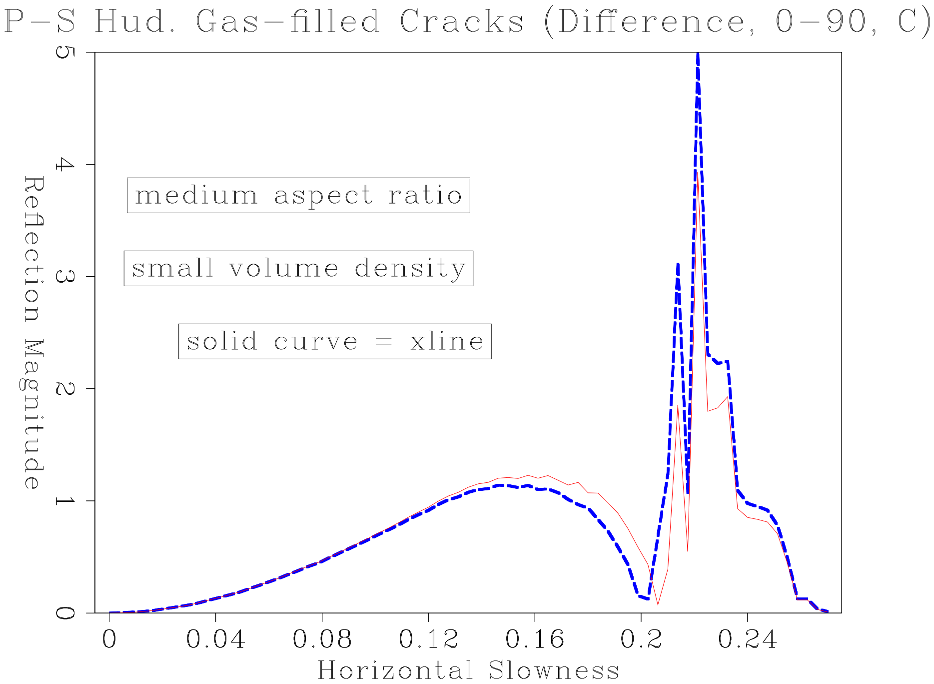

Figure 27: PS reflection amplitude comparison of inline and crossline for dry cracks type of C. martin1-comp.C.huddry.ps.tp [NR]

behaviour. All our measurements are with respect to a fixed azimuth, that serves as a reference. Variations from that reference can indicate anisotropy due to fracture orientation and fracture content. The numerical modeling examples we showed above should be taken as a lower crack density bound, since they are based on a small volume density of cracks. Austin chalk may exhibit stronger fracturing in reality.

CONCLUSIONS

Reflection amplitude modeling analysis for anisotropic media is carried out in the $\tau - p$ domain. Working in the "phase" domain allows a robust estimate of reflection amplitudes. Interfering and triplicating events are handled accurately. The travel-time curve in the "phase" domain relates directly to the inverse of the phase slowness surface of the medium. Within the validity of crack models used, inline-crossline velocity anisotropy varies from 0-15 percent. However, the reflection amplitude exhibits a smaller degree of variation, typically less than 10 percent. The reflection response depends on the material filling the cracks, the crack shape, and the crack density. We used methane, water, and vacuum for filling materials. The PP reflection magnitude is affected greatest between P and S critical angles. The PS reflection coefficient seems to exhibit anisotropy over a larger angular range independent of the filling material. PS converted mode reflection seems more sensitive in attempting to distinguish gas- and fluid-filled fractures together with their orientations.

REFERENCES

Cunha, C., 1991, Angle-dependent reflectivity from elastic reverse time migration: SEP–**72**, 111–122.

Dellinger, J., Muir, F., and Karrenbach, M., 1992, Anelliptic approximations for TI media: SEP–**75**, 333–354.

Kostov, C., 1990, Seismic signals from a drillbit source: Ph.D. thesis, Stanford University.

Nichols, D., 1989, A comparison of two models for the elastic properties of fractured rock: SEP–**60**, 261–270.

Nichols, D., 1992, Dealiasing bandlimited data using a spectral continuity constraint: SEP–**73**, 161–184.

Ostrander, W. J., 1984, Plane-wave reflection coefficients for gas sands at nonnormal angles-of-incidence: Geophysics, **49**, no. 10, 1637–1648.

Schoenberg, M., and Muir, F., 1989, A calculus for finely layered anisotropic media: Geophysics, **54**, no. 5, 581–589.

White, J. E., 1982, Computed waveforms in transversely isotropic media: Geophysics, **47**, no. 5, 771–783.

Wright, J., 1987, The effects of transverse isotropy on reflection amplitude versus offset (short note): Geophysics, **52**, no. 4, 564–567.

APPENDIX A

For comparing the azimuthal AVO responses we used the following elastic constants in units of $[10^9 N/m^2]$:

medium type	c11	c12	c13	c22	c23	c33	c44	c55	c66	ρ
huddry inline	61.5	21.75	21.75	43.5	21.75	61.5	15.075	16.875	15.075	2.7
huddry xline	43.5	21.75	21.75	61.5	32.755	61.5	16.875	15.075	15.075	2.7
hudwet inline	66.51	31.76	32.76	63.52	31.76	66.51	15.075	16.875	15.075	2.7
hudwet xline	63.52	31.76	31.76	66.505	31.76	66.505	16.875	15.075	15.075	2.7
A fluid inline	65.793	30.34	32.34	60.67	30.34	65.793	15.075	16.8750	15.075	2.7
A fluid xline	60.72	30.34	30.34	65.79	32.04	60.72	16.875	15.075	15.075	2.7
B fluid inline	67.27	33.29	33.52	66.58	33.29	66.27	15.075	16.875	15.075	2.7
B fluid xline	66.587	33.29	33.52	67.27	33.52	66.27	16.875	15.075	15.075	2.7
C gas inline	66.30	31.35	32.55	62.70	31.35	66.30	16.515	16.875	16.515	2.7
C gas xline	62.7	31.35	31.35	66.3	32.55	66.30	16.875	16.515	16.515	2.7
C fluid inline	66.30	31.35	32.55	62.70	31.35	66.30	16.515	16.875	16.515	2.7
C fluid xline	62.7	31.35	31.35	66.3	32.55	66.30	16.875	16.515	16.515	2.7